Acta Mech 226, 2295–2311 (2015)
DOI 10.1007/s00707-015-1311-9

Jia-Jia Mao · Liao-Liang Ke · Yue-Sheng Wang

Thermoelastic instability of functionally graded materials in frictionless contact

Received: 30 October 2014 / Revised: 16 December 2014 / Published online: 20 February 2015

Abstract This paper investigates the static thermoelastic instability between a functionally graded material (FGM) half-plane and a homogeneous half-plane under the plane strain state using the perturbation method. Two frictionless half-planes are pressed together by a uniform pressure and transmit a uniform heat flux at their interface where a pressure-dependent thermal contact resistance is taken into account. The material properties of the FGMs are assumed to be of an exponential form. The characteristic equation is derived to determine the thermoelastic instability behavior of two half-planes. The instabilities are categorized into three types based on the ratio of the material properties. The effects of the gradient index, thermal contact resistance and material combination on the critical heat flux are discussed by the parametric studies. It is indicated that the use of FGMs can improve the thermoelastic instability behavior of systems.

1 Introduction

Functionally graded materials (FGMs) are materials that comprise a spatial gradient in structure and/or composition, tailored for a specific performance or function. They can reduce the magnitude of residual and thermal stresses, mitigate stress concentration and increase fracture toughness [1]. In the past few years, many experimental and numerical results have shown that controlling a material property gradient in FGMs could lead to a significant improvement in the resistance to the contact deformation and damage [2–12]. This potential application motivates the study of the contact mechanics of FGMs.

FGMs are often required to service in thermal environments where the heat conduction will inevitably affect the contact behavior of FGMs. Generally, there are two important topics of thermoelastic contact problems. One is the thermoelastic contact stress analysis of FGMs subjected to thermomechanical loads. Choi and Paulino [13] analyzed the thermoelastic contact problem between a rigid flat punch and an FGM coating/substrate system. Barik et al. [14] concerned a functionally graded heat-conducting punch sliding over a rigid insulated half-plane. Shahzamanian et al. [15,16] presented the contact analysis of an FGM brake disk and found that the gradient of the metal–ceramic FGMs has significant effects on the thermomechanical response of the FGM brake disk. Liu et al. [17,18] analyzed the thermoelastic contact of FGMs with exponentially or arbitrarily varying properties. Their results showed that the distribution of the contact stress and surface temperature can be altered by adjusting the gradient index, Peclet number and friction coefficient. Recently, Chen and Chen [19] presented the thermoelastic contact of a finite graded layer under a sliding rigid punch with frictional heat generation. They discussed the distributions of the contact pressure and the in-plane stress under the prescribed thermoelastic environment with different parameter combinations, including ratio of shear modulus, relative sliding speed, friction coefficient and thermal parameters in detail.

J.-J. Mao · L.-L. Ke (✉) · Y.-S. Wang
Institute of Engineering Mechanics, Beijing Jiaotong University, Beijing 100044, People's Republic of China
E-mail: llke@bjtu.edu.cn
Tel.: +86-10-51685755
Fax: +86-10-51682094

The other topic is the thermoelastic contact instability problem of FGMs. Generally, this problem can be considered as two major categories, namely the frictionally excited thermoelastic instability in a sliding contact system involving the frictional heat and the static thermoelastic instability due to the pressure-dependent thermal contact resistance when the heat flux transfers across the contact interface. For these two categories of thermoelastic instability problems, "instability" means that if the conducting heat flux or sliding speed between two bodies is sufficiently high, both steady-state and transient solutions can be unstable in the sense that an arbitrarily small perturbation in the initial condition can cause large changes in the subsequent behavior and finally result in the thermoelastic contact. As pointed out by Li [20], the system tends to a steady oscillatory state in which the contact pressure varies periodically with time, leading possibly to periodic separation if the instability occurs. Jang and his co-authors presented comprehensive studies on the frictionally excited thermoelastic instability of FGMs, such as a stationary FGM layer between two sliding homogeneous layers [21], an FGM half-plane sliding against a homogeneous half-plane [22], and an FGM layer sliding against two homogeneous half-planes [23]. Their studies revealed that an optimal gradient index of FGMs can lead to a maximum critical speed and enhance the performance of the frictional sliding system. Hernik [24] considered the application of functionally graded A356R-based composite to the brake disk structure in order to prevent the thermoelastic instability of the braking system. However, the works on the static thermoelastic instability are quite limited despite their importance in the design of FGM structures. So far, only Mao et al. [25] investigated the static thermoelastic instability of an FGM layer and a homogeneous half-plane. It is not enough to understand the static thermoelastic stability behaviors of FGMs used in different structural systems. Therefore, we should make further studies on some fundamental problems of the static thermoelastic instability of FGMs, such as the contact between two frictionless half-planes, two frictionless layers, two bonded half-planes, and two bonded layers, because these systems will show different stability behaviors from each other.

For homogeneous materials, two categories of thermoelastic contact instability problems have been extensively studied by many investigators, especially by Barber and his co-authors. By using the perturbation method, Lee and Barber [26] investigated the frictionally excited thermoelastic instability for a layer with finite thickness sliding between two half-planes pressed by a uniform pressure. Yi et al. [27] proposed the Fourier reduction method to obtain an efficient solution of the frictional thermoelastic stability problem for systems with two sliding bodies. Lee [28] studied the frictionally excited thermoelastic instability in automotive drum brake systems with one side frictional heating model. The effect of the friction coefficient and brake material properties on the critical speed was examined. Afferrante et al. [29] analyzed the transient thermoelastic stability behavior in a thin layer sliding between two half-planes. Ahn and Jang [30] discussed the thermoelastic–plastic instability in the frictional sliding system by using the transient finite element simulation. For the static thermoelastic instability problems, Barber [31] first studied the stability of nominally uniform contact between two elastic half-planes by assuming the pressure-dependent thermal contact resistance. Zhang and Barber [32] examined the influence of material properties on the stability criterion for the contact between two half-planes. They classified the material combinations into five categories on the basis of the ratios of material properties. Yeo and Barber [33] focused on the effect of finite geometry on the stability of the thermoelastic contact between a layer and a half-plane. Li and Barber [34] discussed the thermoelastic stability of a system consisting of two layers in contact by using the perturbation method. Specially, Ciavarella and his co-authors considered the simultaneous frictionally excited and static thermoelastic instabilities, such as an elastic conducting half-plane sliding against a rigid perfect conductor wall [35], two half-planes sliding out-of-plane [36], and a rectangular elastic block sliding against a rigid wall [37].

In this paper, the static thermoelastic contact instability between an FGM half-plane and a homogeneous half-plane under the plane strain state is studied by using the perturbation method. Two frictionless half-planes are pressed together by a uniform pressure and transmit a uniform heat flux at the interface where a pressure-dependent thermal contact resistance is considered because of the imperfect contact between two half-planes. The material properties of FGMs are assumed to be of an exponential form. The characteristic equation is obtained to determine the stability boundary for three types of material combinations. The effects of the gradient index, thermal contact resistance and material combination on the critical heat flux are examined.

2 Formulation of the thermoelastic instability problem

Figure 1 shows the thermoelastic frictionless contact problem between an FGM half-plane ($y > 0$) and a homogeneous half-plane ($y < 0$) pressed together by a uniform pressure p_0. A uniform heat flux $q_y = q_0$ in the positive y-direction is transmitted over their interface $y = 0$. It is assumed that the thermoelastic properties of the FGM half-plane change continuously along the y-direction according to the exponential function

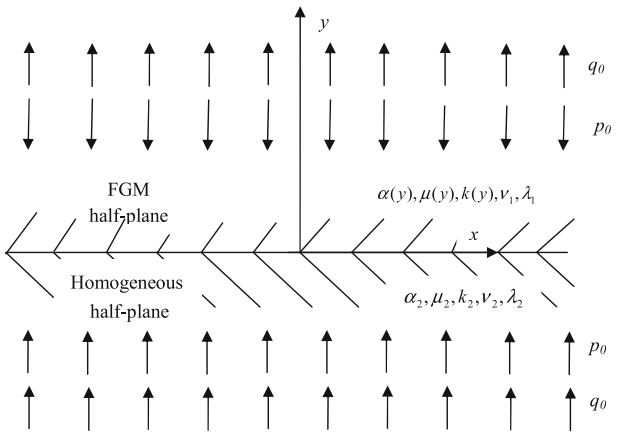

Fig. 1 An FGM half-plane on a homogeneous half-plane pressed by a uniform pressure and transmitting a uniform heat flux

$$\mu(y) = \mu_b e^{\beta y},\ k(y) = k_b e^{\delta y},\ \alpha(y) = \alpha_b e^{\gamma y},\ c(y) = c_b e^{\varepsilon y},\ \rho(y) = \rho_b e^{\varsigma y} \tag{1}$$

where $\mu(y)$, $k(y)$, $\alpha(y)$, $c(y)$ and $\rho(y)$ are the shear modulus, thermal conductivity coefficient, thermal expansion coefficient, specific heat and mass density, respectively; β, δ, γ, ε and ς are the gradient indexes; the Poisson's ratio v is assumed as constant for simplicity; $\mu_b, k_b, \alpha_b, c_b$ and ρ_b are the thermoelastic properties at the surface ($y = 0$) of the FGM half-plane.

2.1 Temperature perturbation

Refer to [26], the temperature perturbation in each half-plane can be written in the form as

$$T_j(x, y, t) = f_j(y)\, e^{bt + imx}, \quad j = 1, 2 \tag{2}$$

where $i = \sqrt{-1}$; subscripts "1" and "2" refer to the FGM half-plane and the homogeneous half-plane, respectively; $f_j(y)$ are complex functions of the real variable y that are determined by satisfying the transient heat conduction equation; m is the wave number; and b is the exponential growth rate. The exponential growth rate b can be either real or complex. Instability may occur if solutions exist with a positive real b or a complex b with a positive real part [32].

The temperature perturbation must satisfy the transient heat conduction equation

$$\frac{\partial^2 T_1}{\partial x^2} + \frac{\partial^2 T_1}{\partial y^2} + \delta \frac{\partial T_1}{\partial y} = \frac{1}{\lambda_1} \frac{\partial T_1}{\partial t} \tag{3}$$

for the FGM half-plane, and

$$\frac{\partial^2 T_2}{\partial x^2} + \frac{\partial^2 T_2}{\partial y^2} = \frac{1}{\lambda_2} \frac{\partial T_2}{\partial t} \tag{4}$$

for the homogenous half-plane, where $\lambda_j = k_j/\rho_j c_j$ $(j = 1, 2)$ are the thermal diffusivity coefficients of the FGM half-plane and the homogeneous half-plane, respectively. Although the thermal diffusivity coefficient changes with the location in the FGM half-plane, we assume that the gradient indexes of thermal conductivity, density and specific heat have the relation of $\delta = \varepsilon + \varsigma$ in order to obtain a constant thermal diffusivity coefficient. Hence, it is possible to solve Eq. (3) analytically. Note that Liu et al. [17] analyzed the effect of the thermal diffusivity coefficient on the thermoelastic contact stress of FGMs. Their results indicated that the graded variation of the thermal diffusivity coefficient has a slight effect on the thermoelastic fields. Therefore, it is reasonable to assume a constant thermal diffusivity coefficient in the present paper.

Substituting Eq. (2) into Eq. (3), we obtain the temperature perturbation for the FGM half-plane, which must decay away from the interface, i.e., $T_1 \to 0$ as $y \to +\infty$. Thus, we have

$$T_1(x, y, t) = C_{11} e^{\eta_{11} y} e^{bt + imx} \tag{5}$$

where C_{11} is an unknown constant to be determined; and

$$\eta_{11} = \frac{1}{2}\left[-\delta - \sqrt{\delta^2 + 4\left(m^2 + \frac{b}{\lambda_1}\right)}\right]. \tag{6}$$

Similarly, substituting Eq. (2) into Eq. (4) yields the temperature perturbation for the homogenous half-plane,

$$T_2(x, y, t) = C_{21} \mathrm{e}^{\eta_{21} y} \mathrm{e}^{bt + \mathrm{i}mx}, \tag{7}$$

where C_{21} is an unknown constant; and

$$\eta_{21} = \sqrt{m^2 + \frac{b}{\lambda_2}}. \tag{8}$$

2.2 Thermoelastic stress and displacement fields

For both half-planes, the governing equations for the linear isotropic elastic solid in the plane strain state can be written as

$$\nabla^2 u_{xj} + \frac{2}{\Theta_j - 1}\left(\frac{\partial^2 u_{xj}}{\partial x^2} + \frac{\partial^2 u_{yj}}{\partial x \partial y}\right) + \beta\left(\frac{\partial u_{xj}}{\partial y} + \frac{\partial u_{yj}}{\partial x}\right) = \frac{4\bar{\alpha}_j \mathrm{e}^{\gamma y}}{\Theta_j - 1}\frac{\partial T_j}{\partial x}, \tag{9}$$

$$\nabla^2 u_{yj} + \frac{2}{\Theta_j - 1}\left(\frac{\partial^2 u_{yj}}{\partial y^2} + \frac{\partial^2 u_{xj}}{\partial x \partial y}\right) + \frac{\beta}{\Theta_j - 1}\left[\left(1 + \Theta_j\right)\frac{\partial u_{yj}}{\partial y} + \left(3 - \Theta_j\right)\frac{\partial u_{xj}}{\partial x}\right] = \frac{4\bar{\alpha}_j \mathrm{e}^{\gamma y}}{\Theta_j - 1}\left[\left(\beta + \gamma\right) T_j + \frac{\partial T_j}{\partial y}\right] \tag{10}$$

where $j = 1, 2$; $u_{xj} = u_{xj}(x, y, t)$ and $u_{yj} = u_{yj}(x, y, t)$ are the displacements in the x- and y-directions, respectively; and

$$\bar{\alpha}_1 = \alpha_{\mathrm{b}}(1 + \nu_1),\ \bar{\alpha}_2 = \alpha_2(1 + \nu_2),\ \Theta_j = 3 - 4\nu_j, \tag{11}$$

with ν_1 and ν_2 corresponding to the Poisson's ratios of the FGM half-plane and the homogeneous half-plane, respectively. Note that the governing equations for the homogeneous half-plane can be obtained from Eqs. (9) and (10) by setting $\delta = 0,\ \beta = 0, \gamma = 0$ and $j = 2$.

Similarly, we can write the displacement fields in the perturbation form as

$$u_{xj}(x, y, t) = U_{xj}(y)\, \mathrm{e}^{bt + \mathrm{i}mx}, \tag{12}$$

$$u_{yj}(x, y, t) = U_{yj}(y)\, \mathrm{e}^{bt + \mathrm{i}mx} \tag{13}$$

where $U_{xj}(y)$ and $U_{yj}(y)$ are complex functions of the real variable y.

2.2.1 The FGM half-plane

For the FGM half-plane, the constitutive relations are written as

$$\sigma_{y1} = \frac{\left(\Theta_1 + 1\right)\mu_{\mathrm{b}} \mathrm{e}^{\beta y}}{\Theta_1 - 1}\left(\frac{\partial u_{y1}}{\partial y} - \frac{\Theta_1 - 3}{\Theta_1 + 1}\frac{\partial u_{x1}}{\partial x}\right) - \frac{4\mu_{\mathrm{b}}\bar{\alpha}_1 \mathrm{e}^{(\beta+\gamma)y}}{\Theta_1 - 1} T_1, \tag{14}$$

$$\sigma_{xy1} = \mu_{\mathrm{b}} \mathrm{e}^{\beta y}\left(\frac{\partial u_{y1}}{\partial x} + \frac{\partial u_{x1}}{\partial y}\right). \tag{15}$$

Substituting Eqs. (5), (12) and (13) into Eqs. (9) and (10), we obtain

$$U''_{x1}(y)+\beta U'_{x1}(y)-\frac{\Theta_1+1}{\Theta_1-1}m^2U_{x1}(y)+\mathrm{i}m\left[\beta U_{y1}(y)+\frac{2}{\Theta_1-1}U'_{y1}(y)\right]$$
$$=\mathrm{i}m\frac{4\bar{\alpha}_1C_{11}\mathrm{e}^{(\gamma+\eta_{11})y}}{\Theta_1-1}, \tag{16}$$

$$\frac{\Theta_1+1}{\Theta_1-1}U''_{y1}(y)+\beta\frac{\Theta_1+1}{\Theta_1-1}U'_{y1}(y)-m^2U_{y1}(y)+\frac{\mathrm{i}m}{\Theta_1-1}\left[\beta(3-\Theta_1)U_{x1}(y)+2U'_{x1}(y)\right]$$
$$=\frac{4\bar{\alpha}_1\mathrm{e}^{(\gamma+\eta_{11})y}}{\Theta_1-1}(\beta+\gamma+\eta_{11})C_{11}. \tag{17}$$

The solutions of the ordinary differential equations (16) and (17), which are composed of the homogeneous solution and the particular solution, can be expressed as

$$U_{x1}(y)=A_{11}\mathrm{e}^{f_{11}y}+A_{12}\mathrm{e}^{f_{12}y}+A_{13}\mathrm{e}^{(\gamma+\eta_{11})y}, \tag{18}$$
$$U_{y1}(y)=B_{11}\mathrm{e}^{f_{11}y}+B_{12}\mathrm{e}^{f_{12}y}+B_{13}\mathrm{e}^{(\gamma+\eta_{11})y} \tag{19}$$

where A_{11}, A_{12}, A_{13}, B_{11}, B_{12} and B_{13} are the unknowns to be determined from the boundary conditions; and

$$f_{11}=\frac{1}{2}\left[-\beta-\sqrt{4m^2+\beta^2-4\mathrm{i}m\beta\sqrt{\frac{3-\Theta_1}{\Theta_1+1}}}\right],\quad f_{12}=\frac{1}{2}\left[-\beta-\sqrt{4m^2+\beta^2+4\mathrm{i}m\beta\sqrt{\frac{3-\Theta_1}{\Theta_1+1}}}\right], \tag{20}$$

$$B_{1j}=\mathrm{i}s_jA_{1j},s_j=\frac{\left(f_{1j}^2+\beta f_{1j}\right)(\Theta_1-1)-m^2(\Theta_1+1)}{\left[2f_{1j}+\beta(\Theta_1-1)\right]m},\quad j=1,2, \tag{21}$$

$$B_{13}=\frac{M_2A_{13}}{\mathrm{i}mM_1},\quad C_{11}=\frac{(\Theta_1-1)A_{13}}{4\mathrm{i}m\bar{\alpha}_1M_1}, \tag{22}$$

$$M_1=\frac{P-\left[Q+\frac{2(\Theta_1-2)}{(\Theta_1-1)}\beta\right](\beta+\gamma+\eta_{11})}{P\left[\frac{\Theta_1-1}{\Theta_1+1}P-\frac{4\Theta_1m^2}{\Theta_1^2-1}\right]+m^2Q\left[Q+\frac{2(\Theta_1-2)}{\Theta_1-1}\beta\right]}, \tag{23}$$

$$M_2=\frac{(\beta+\gamma+\eta_{11})\left[\frac{\Theta_1-1}{\Theta_1+1}P-\frac{4\Theta_1m^2}{\Theta_1^2-1}\right]+m^2Q}{P\left[\frac{\Theta_1-1}{\Theta_1+1}P-\frac{4\Theta_1m^2}{\Theta_1^2-1}\right]+m^2Q\left[Q+\frac{2(\Theta_1-2)}{\Theta_1-1}\beta\right]}, \tag{24}$$

$$P=\frac{\Theta_1+1}{\Theta_1-1}(\gamma+\eta_{11})^2+\beta\frac{\Theta_1+1}{\Theta_1-1}(\gamma+\eta_{11})-m^2,\quad Q=\beta\frac{3-\Theta_1}{\Theta_1-1}+\frac{2}{\Theta_1-1}(\gamma+\eta_{11}). \tag{25}$$

Then, the displacements of the FGM half-plane can be further expressed as

$$u_{x1}(x,y,t)=\left[A_{11}\mathrm{e}^{f_{11}y}+A_{12}\mathrm{e}^{f_{12}y}+A_{13}\mathrm{e}^{(\gamma+\eta_{11})y}\right]\mathrm{e}^{bt+\mathrm{i}mx}, \tag{26}$$

$$u_{y1}(x,y,t)=\left[\mathrm{i}s_1A_{11}\mathrm{e}^{f_{11}y}+\mathrm{i}s_2A_{12}\mathrm{e}^{f_{12}y}+\frac{M_2}{\mathrm{i}mM_1}A_{13}\mathrm{e}^{(\gamma+\eta_{11})y}\right]\mathrm{e}^{bt+\mathrm{i}mx}. \tag{27}$$

By substituting Eqs. (26) and (27) into Eqs. (14) and (15), we obtain the stress fields of the FGM half-plane as

$$\sigma_{y1}(x,y,t)=\left\{\frac{\mu_{\mathrm{b}}\mathrm{e}^{\beta y}}{\Theta_1-1}\sum_{j=1}^{2}\left[\mathrm{i}s_j f_{1j}\left(\Theta_1+1\right)+\mathrm{i}m\left(3-\Theta_1\right)\right]A_{1j}\mathrm{e}^{f_{1j}y}\right.$$
$$\left.+\left[\frac{i\mu_{\mathrm{b}}}{mM_1}-\frac{\mathrm{i}\left(\Theta_1+1\right)\mu_{\mathrm{b}}M_2\left(\gamma+\eta_{11}\right)}{\left(\Theta_1-1\right)mM_1}-\frac{\mathrm{i}m\left(\Theta_1-3\right)\mu_{\mathrm{b}}}{\Theta_1-1}\right]A_{13}\mathrm{e}^{(\beta+\gamma+\eta_{11})y}\right\}\mathrm{e}^{bt+\mathrm{i}mx}, \tag{28}$$

$$\sigma_{xy1}(x,y,t)=\mu_{\mathrm{b}}\mathrm{e}^{\beta y}\left[\sum_{j=1}^{2}\left(f_{1j}-ms_j\right)\mathrm{e}^{f_{1j}y}A_{1j}+\left(\gamma+\eta_{11}+\frac{M_2}{M_1}\right)\mathrm{e}^{(\gamma+\eta_{11})y}A_{13}\right]\mathrm{e}^{bt+\mathrm{i}mx}. \tag{29}$$

2.2.2 The homogeneous half-plane

For the homogeneous half-plane, the constitutive relations are given by

$$\sigma_{y2}=\frac{\left(\Theta_2+1\right)\mu_2}{\Theta_2-1}\left(\frac{\partial u_{y2}}{\partial y}-\frac{\Theta_2-3}{\Theta_2+1}\frac{\partial u_{x2}}{\partial x}\right)-\frac{4\mu_2\bar{\alpha}_2}{\Theta_2-1}T_2, \tag{30}$$

$$\sigma_{xy2}=\mu_2\left(\frac{\partial u_{y2}}{\partial x}+\frac{\partial u_{x2}}{\partial y}\right). \tag{31}$$

Substituting Eqs. (7), (12) and (13) into Eqs. (9) and (10) and setting $\delta=\beta=\gamma=0$ yield

$$U_{x2}''(y)-\frac{\Theta_2+1}{\Theta_2-1}m^2U_{x2}(y)+\frac{2\mathrm{i}m}{\Theta_2-1}U_{y2}'(y)=\frac{4\mathrm{i}m\bar{\alpha}_2}{\Theta_2-1}C_{21}\mathrm{e}^{\eta_{21}y}, \tag{32}$$

$$\frac{\Theta_2+1}{\Theta_2-1}U_{y2}''(y)-m^2U_{y2}(y)+\frac{2\mathrm{i}m}{\Theta_2-1}U_{x2}'(y)=\frac{4\eta_{21}\bar{\alpha}_2}{\Theta_2-1}C_{21}\mathrm{e}^{\eta_{21}y}. \tag{33}$$

The solutions of Eqs. (32) and (33) are expressed as

$$U_{x2}\left(y\right)=\left(A_{21}+A_{22}y\right)\mathrm{e}^{my}+A_{23}\mathrm{e}^{\eta_{21}y},\quad U_{y2}\left(y\right)=\left(B_{21}+B_{22}y\right)\mathrm{e}^{my}+B_{23}\mathrm{e}^{\eta_{21}y} \tag{34}$$

where

$$B_{21}=-\mathrm{i}A_{21}+\frac{\mathrm{i}\Theta_2}{m}A_{22},\quad B_{22}=-\mathrm{i}A_{22}, \tag{35}$$

$$B_{23}=-\frac{\mathrm{i}\eta_{21}}{m}A_{23},\quad C_{21}=\frac{\left(\eta_{21}^2-m^2\right)\left(\Theta_2+1\right)}{4\mathrm{i}m\bar{\alpha}_2}A_{23} \tag{36}$$

with A_{21}, A_{22}, and A_{23} being unknowns to be determined by the boundary conditions.

The displacement fields, which satisfy the regularity conditions $u_{x2}\left(x,-\infty,t\right)=0$ and $u_{y2}\left(x,-\infty,t\right)=0$ are obtained as

$$u_{x2}(x,y,t)=\left[\left(A_{21}+A_{22}y\right)\mathrm{e}^{my}+A_{23}\mathrm{e}^{\eta_{21}y}\right]\mathrm{e}^{bt+\mathrm{i}mx}, \tag{37}$$

$$u_{y2}(x,y,t)=\left\{-\mathrm{i}\left[A_{21}+\left(y-\frac{\Theta_2}{m}\right)A_{22}\right]\mathrm{e}^{my}-\frac{\mathrm{i}\eta_{21}}{m}A_{23}\mathrm{e}^{\eta_{21}y}\right\}\mathrm{e}^{bt+\mathrm{i}mx}. \tag{38}$$

Then, the stress fields of the homogeneous half-plane are

$$\sigma_{y2}(x,y,t)=\left\{2\mathrm{i}\mu_2\left[-mA_{21}+\left(\frac{1+\Theta_2}{2}-my\right)A_{22}\right]\mathrm{e}^{my}-2\mathrm{i}\mu_2mA_{23}\mathrm{e}^{\eta_{21}y}\right\}\mathrm{e}^{bt+\mathrm{i}mx}, \tag{39}$$

$$\sigma_{xy2}(x,y,t)=\left\{2\mu_2\left[mA_{21}+\left(\frac{1-\Theta_2}{2}+my\right)A_{22}\right]\mathrm{e}^{my}+2\mu_2\eta_{21}\mathrm{e}^{\eta_{21}y}A_{23}\right\}\mathrm{e}^{bt+\mathrm{i}mx}. \tag{40}$$

2.3 Boundary conditions

It is assumed that the contact is frictionless and the heat flux, stress and displacement are continuous at the interface $y = 0$. Then, we have

$$\sigma_{xy1}(x,0,t) = \sigma_{xy2}(x,0,t) = 0, \quad \sigma_{y1}(x,0,t) = \sigma_{y2}(x,0,t), \tag{41}$$

$$u_{y1}(x,0,t) = u_{y2}(x,0,t), \quad q_1(x,0,t) = q_2(x,0,t) \tag{42}$$

where

$$q_1(x,y,t) = -k_b e^{\delta y}\frac{\partial T_1(x,y,t)}{\partial y} = \mathrm{i}k_b\eta_{11}\frac{\Theta_1 - 1}{4m\bar{\alpha}_1 M_1}A_{13}e^{(\delta+\eta_{11})y}e^{bt+\mathrm{i}mx}, \tag{43}$$

$$q_2(x,y,t) = -k_2\frac{\partial T_2(x,y,t)}{\partial y} = \mathrm{i}k_2\eta_{21}\frac{\left(\eta_{21}^2 - m^2\right)(\Theta_2+1)}{4m\bar{\alpha}_2}A_{23}e^{\eta_{21}y}e^{bt+\mathrm{i}mx}. \tag{44}$$

Note that the above boundary conditions (41) and (42) can lead to a system of five equations, which is not sufficient to be solved for six unknowns—A_{11}, A_{12}, A_{13}, A_{21}, A_{22} and A_{23}. We must add an additional equation to determine these unknowns. In the present problem, the sixth equation can be acquired according to the perturbation of the thermal contact resistance relation.

2.4 Perturbation of the thermal contact resistance relation

Due to the imperfect contact between two half-planes, a pressure-dependent contact thermal resistance R at the interface is defined as [31]

$$q_y = \frac{T^*}{R(p)} \tag{45}$$

where T^* is the temperature drop across the interface. Hence, for small perturbations under the steady state [31], we have

$$R_0\Delta q + q_0\Delta R = \Delta T \tag{46}$$

where

$$\Delta R = R'\Delta p, \quad R_0 = R(p_0), \tag{47}$$

with $R' = \mathrm{d}R(p)/\mathrm{d}p$; and Δp, ΔT and Δq are the perturbations in the contact pressure, temperature difference and heat flux at the interface $y = 0$, respectively. Their expressions can be formulated as

$$\Delta p = -\sigma_{y2}(x,0,t) = -\left[2\mathrm{i}\mu_2\left(-mA_{21} + \frac{1+\Theta_2}{2}A_{22}\right) - 2\mathrm{i}\mu_2 mA_{23}\right]e^{bt+\mathrm{i}mx}, \tag{48}$$

$$\Delta T = T_2(x,0,t) - T_1(x,0,t) = \left[\frac{\left(\eta_{21}^2 - m^2\right)(\Theta_2+1)}{4\mathrm{i}m\bar{\alpha}_2}A_{23} - \frac{\Theta_1 - 1}{4\mathrm{i}m\bar{\alpha}_1 M_1}A_{13}\right]e^{bt+\mathrm{i}mx}, \tag{49}$$

$$\Delta q = q_2(x,0,t) = \mathrm{i}k_2\eta_{21}\frac{\left(\eta_{21}^2 - m^2\right)(\Theta_2+1)}{4m\bar{\alpha}_2}A_{23}e^{bt+\mathrm{i}mx}. \tag{50}$$

Substitution of Eqs. (48)–(50) into Eq. (46) yields

$$\begin{aligned} &-\tfrac{\Theta_1-1}{4m\bar{\alpha}_1 M_1}A_{13} + 2mq_0\mu_2 R'A_{21} - q_0\mu_2(\Theta_2+1)R'A_{22} \\ &+\left[\tfrac{\left(\eta_{21}^2-m^2\right)(\Theta_2+1)(1+k_2\eta_{21}R_0)}{4m\bar{\alpha}_2} + 2mq_0\mu_2 R'\right]A_{23} = 0 \end{aligned}. \tag{51}$$

Equation (51) together with the boundary conditions (41) and (42) can lead to a system of six linear homogeneous equations for six unknowns—A_{11}, A_{12}, A_{13}, A_{21}, A_{22} and A_{23}. For the non-trivial solution, the

determinant of the coefficient matrix of these six equations must be zero. Thus, we can obtain the characteristic equation for the exponential growth rate b as

$$\mathbf{det}\left[\{g_{1i}\},\{g_{2i}\},\{g_{3i}\},\{g_{4i}\},\{g_{5i}\},\{g_{6i}\}\right]^{\mathrm{T}}=0, \tag{52}$$

where $i=1,2,\cdots,6$; the superscript "T" denotes the transposition of a matrix, and $\{g_{1i}\},\cdots,\{g_{6i}\}$ are given in Appendix A.

Introduce the following dimensionless parameters:

$$\beta^*=\frac{\beta}{m},\quad \delta^*=\frac{\delta}{m},\quad \gamma^*=\frac{\gamma}{m}, r_1=\frac{\lambda_2}{\lambda_1},\quad r_2=\frac{\bar{\alpha}_2}{\bar{\alpha}_1},\quad r_3=\frac{k_2}{k_\mathrm{b}},\quad r_4=\frac{\mu_2}{\mu_\mathrm{b}},\quad r_5=\frac{\theta_2}{\theta_1}, \tag{53}$$

$$f_{1j}^*=\frac{f_{1j}}{m},\quad (j=1,2),\quad \eta_{11}^*=\frac{\eta_{11}}{m},\quad \eta_{21}^*=\frac{\eta_{21}}{m}=\sqrt{1+\frac{z}{r_1}}, \tag{54}$$

$$P^*=\frac{P}{m^2},\quad Q^*=\frac{Q}{m},\quad M_1^*=m^2M_1,\quad M_2^*=mM_2, \tag{55}$$

$$z=\frac{b}{m^2\lambda_\mathrm{b}},\quad H=mh,\quad R^*=mR_0k_\mathrm{b},\quad Q^*=-4\bar{\alpha}_1q_0R'\Gamma \tag{56}$$

where

$$\Gamma=\frac{2\mu_\mathrm{b}\mu_2}{\mu_2\left(1+\Theta_1\right)+\mu_\mathrm{b}\left(1+\Theta_2\right)},\quad \theta_1=\bar{\alpha}_1/k_\mathrm{b},\quad \theta_2=\bar{\alpha}_2/k_2 \tag{57}$$

Note that θ_j $(j=1,2)$ are generally defined as the distortivity because they relate the thermoelastic distortion to the local heat flux in the steady-state thermal conduction problems [38]. Utilizing the dimensionless parameters, we can write the characteristic equation (52) in dimensionless form as

$$R^*+D_2(H,z)Q^*+D_1(H,z)=0, \tag{58}$$

with

$$D_1(H,z)=-\frac{1}{\eta_{11}^*}+\frac{1}{\eta_{21}^*r_3}, \tag{59}$$

$$D_2(H,z)=\frac{C_1(H,z)}{C_2(H,z)} \tag{60}$$

where $C_1(H,z)$ and $C_2(H,z)$ are given in Appendix B. If we set the gradient index to zero in the FGM half-plane, Eq. (58) can be reduced to the characteristic equation in Ref. [32]. From the characteristic equation (52), we will solve the threshold value of the conducting heat flux which is defined as the critical heat flux.

3 Stability criterion

Instability will occur if the characteristic equation (58) has a solution, either positive or complex with a positive real part, for the dimensionless exponential growth rate $z\left(z=b/m^2\lambda_1\right)$. This instability will be evident when the first root of the characteristic equation passes into the right half complex plane, either through the origin or by crossing the imaginary axis [33]. For the case of a real growth rate, the stability criterion is determined by setting $z=0$. Then, Eq. (58) can be expressed as a linear relation between R^* and Q^*,

$$Q^*=-\frac{R^*+D_1(H,0)}{D_2(H,0)}. \tag{61}$$

For the case of a complex growth rate, the stability criterion is determined by setting $z=\mathrm{i}w$, where w is real. Since both R^* and Q^* must be real, we can solve them by separating real and imaginary parts of Eq. (58) to obtain the following two real equations:

$$R^*+\mathrm{Re}\{D_2\}Q^*+\mathrm{Re}\{D_1\}=0, \tag{62}$$

$$\mathrm{Im}\{D_2\}Q^*+\mathrm{Im}\{D_1\}=0 \tag{63}$$

where

$$Q^*=-\frac{\mathrm{Im}\{D_1\}}{\mathrm{Im}\{D_2\}}, \tag{64}$$

$$R^*=-\mathrm{Re}\{D_2\}Q^*-\mathrm{Re}\{D_1\}. \tag{65}$$

Table 1 Thermoelastic properties of selected materials

Properties	Aluminum alloy	Stainless steel	Nodular cast iron	SiC sintered	Brass	Magnesium alloy
μ (GPa)	27.273	76.923	64.122	172.414	38.372	16.667
α ($^\circ C^{-1}$)	22.0	14.0	13.7	4.4	19.0	26.0
k (W/m °C)	173.0	21.0	48.9	110.0	78.0	95.0
λ (mm^2/s)	67.16	5.93	16.05	35.48	21.35	45.11
ν	0.32	0.30	0.31	0.16	0.33	0.35

4 Results and discussion

In this section, we will discuss the thermoelastic contact instability between an FGM half-plane and a homogeneous half-plane. The effects of the gradient index, thermal contact resistance and classification of material properties on the critical heat flux are demonstrated in Figs. 3, 4, 5, 6, 7, 8 and 9. In order to analyze the effect of various material combinations, the same classification system of Zhang and Barber [31] is also utilized in the present paper, and the first three types of material combinations, i.e., Types 1, 2 and 3 are discussed in detail. We assume that if the dimensionless ratios of material properties satisfy $r_1 > 1$ and $0 < r_5 < 1/r_1$, the system is classified to Type 1; if $r_1 > 1$ and $1/r_1 < r_5 < 1$, the system is Type 2; and if $r_1 > 1$ and $1 < r_5 < r_1$, the system is Type 3.

For the FGM half-plane, the material at the surface is chosen as the nodular cast iron. The FGM half-plane with positive/negative gradients indicates that the material properties exponentially increase/decrease from the surface. For the sake of convenience, the gradient indexes are assumed to be identical, i.e., $\beta^* = \gamma^* = \delta^* = n$, in the following analysis. The materials of the homogenous half-plane are chosen as the SiC sintered for Type 1 ($\theta_1 > \theta_2$), the brass for Type 2 ($\theta_1 > \theta_2$) and the magnesium alloy for Type 3 ($\theta_1 < \theta_2$). Note that the materials with large values of θ generally correspond to materials with great distortivity. The thermoelastic properties of the selected materials, nodular cast iron, SiC, brass and magnesium alloy, are listed in Table 1 [31].

Zhang and Barber [31] investigated the thermoelastic instability between two homogeneous half-planes. If the gradient indexes of the FGM half-plane are set as zero, the present problem can be directly reduced to Zhang and Barber's problem. Figure 2 presents the stability boundaries as a function of R^* for a homogeneous stainless steel half-plane and a homogeneous aluminum alloy half-plane. Zhang and Barber's results are also given in Fig. 2. It is observed that the present results agree well with Zhang and Barber's results.

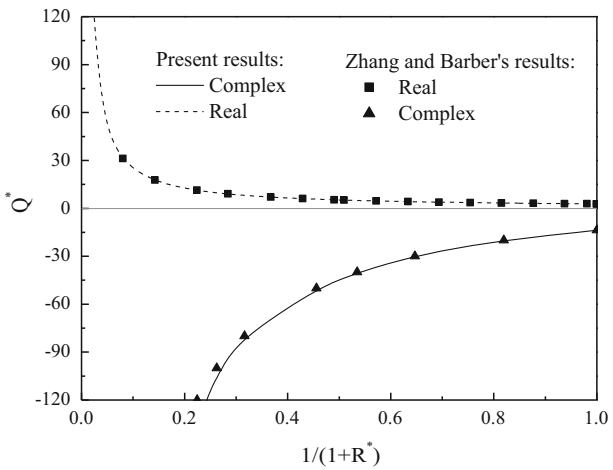

Fig. 2 Stability boundaries as a function of R^* for the contact between two homogeneous half-planes: comparison with existing results

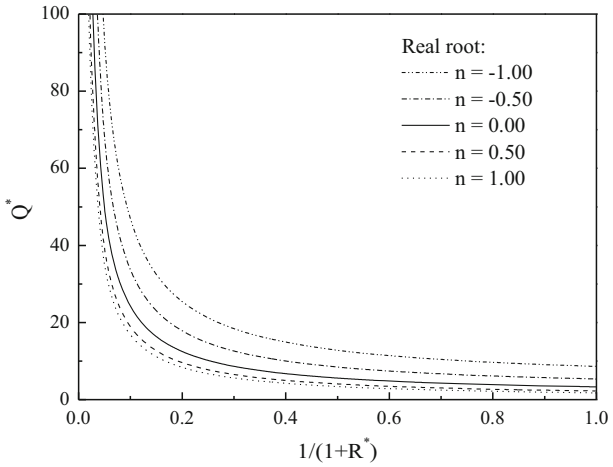

Fig. 3 Stability boundaries as functions of R^* with different gradient indexes n (Type 1)

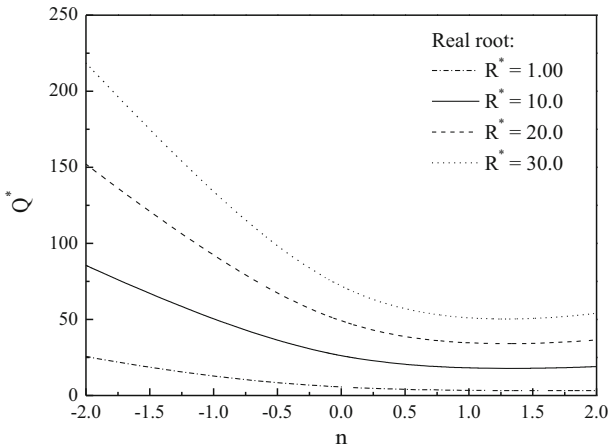

Fig. 4 Stability boundaries as functions of gradient index n with different R^* (Type 1)

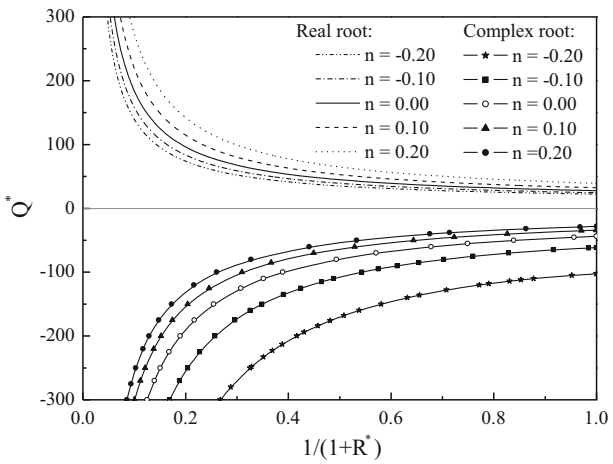

Fig. 5 Stability boundaries as functions of R^* with different gradient indexes n (Type 2)

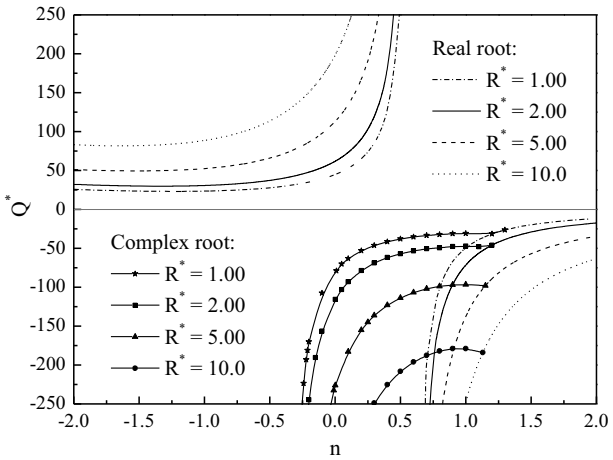

Fig. 6 Stability boundaries as functions of gradient index n with different R^* (Type 2)

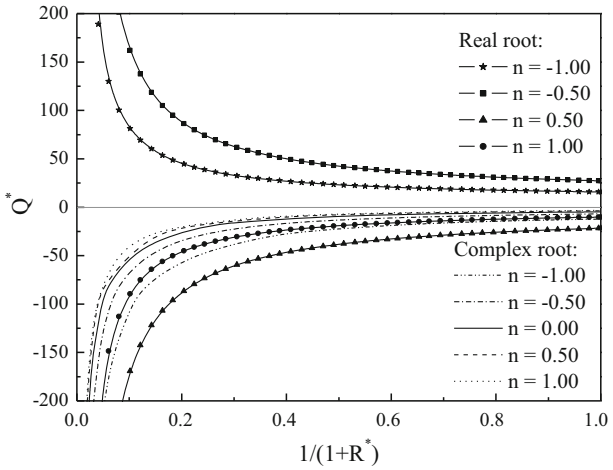

Fig. 7 Stability boundaries as functions of R^* with different gradient index n (Type 3)

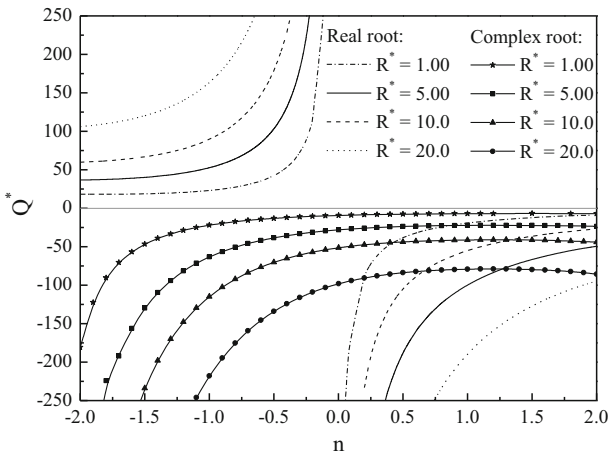

Fig. 8 Stability boundaries as functions of gradient index n with different R^* (Type 3)

4.1 Type 1 material combination

Figure 3 gives the stability boundaries as functions of R^* with different gradient index n. Since R^* can take any positive value, it is convenient to condense the infinite range by plotting Q^* against the function

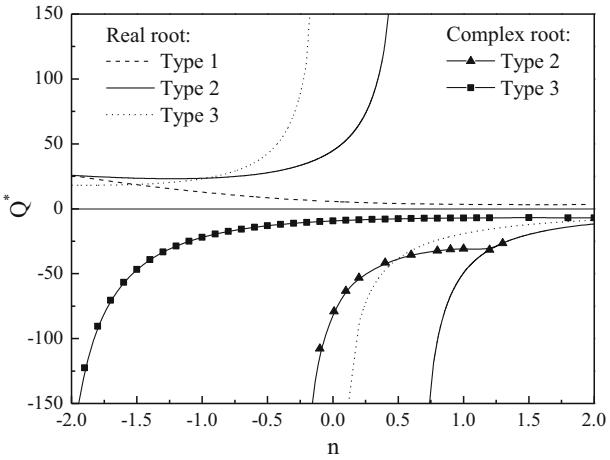

Fig. 9 Effect of the gradient index n on the critical heat flow Q^* for different material combinations with $R^* = 1.0$

$1/(1 + R^*)$, which is always between 0 and 1. The curve of $n = 0$ corresponds to the contact between two homogeneous half-planes. For Type 1 material combination, the stability boundaries can be only determined from the linear real root criterion (61); and instability occurs for the heat flux flowing into the more distortive material (i.e., FGM half-plane, $Q^* > 0$) no matter whether the gradient index is positive or negative. A similar phenomenon was also found by Zhang and Barber [31]. Obviously, the critical heat flux increases with the increase of the thermal contact resistance. This stability behavior is quite different from that of an FGM layer on a homogeneous half-plane studied by Mao et al. [25] where the system can exhibit instability for both directions of the heat flux.

Figure 4 shows the effect of the gradient index n on the critical heat flux Q^* for different dimensionless thermal contact resistances R^*. The critical heat flux decreases rapidly as the gradient index n increases from -2 to 1, and then, it changes slightly as $n \geq 1$. For a given value of n, the bigger the contact resistance R^* is, the more stable the system is. The results imply that we can change the stability boundaries by adjusting the gradient index of FGMs and hence modify the thermoelastic stability behavior of systems.

4.2 Type 2 material combination

Figure 5 plots the stability boundaries as functions of R^* with different values of the gradient index $n(-0.2 \leq n \leq 0.2)$. Dissimilar with Type 1 material combination, instability can occur for both directions of the heat flux for Type 2 material combination. For a smaller gradient index $-0.2 \leq n \leq 0.2$, the critical heat flux is determined from the real root criterion when the heat flux is positive, and increases with the increase of the gradient index. However, the critical heat flux is determined from the complex root criterion when the heat flux is negative, and the absolute value of Q^* decreases with the increase of the gradient index.

Figure 6 examines the effect of the gradient index n on the critical heat flux Q^* for different dimensionless thermal contact resistances R^*. When the heat flux flows into the more distortive material (i.e., FGM half-plane, $Q^* > 0$), the contact is very stable for $n \geq 0.6$. When the heat flux flows into the less distortive material (i.e., homogeneous half-plane, $Q^* < 0$), the critical heat flux is determined from the complex root criterion for the smaller gradient index n(say $n \leq 1.1$), while it is determined from the real root criterion for the lager n (say $n > 1.1$). Furthermore, the contact is very stable for $Q^* < 0$ when the gradient index $n < -0.25$. Similar to Type 1 material combination, the absolute value of the critical heat flux increases with the increase of the thermal contact resistance.

4.3 Type 3 material combination

Figure 7 depicts the stability boundaries as functions of R^* with different values of the gradient index n. For $n < 0$, the system exhibits the real root instability with the positive heat flux and the complex root instability with the negative heat flux. For $n \geq 0$, the system only exhibits the complex root instability with the negative heat flux.

Table 2 Stability behavior for the static thermoelastic contact with $R^* = 1.00$

Material combination	Gradient index n	Critical heat flux	Root
Type 1	$-2.0 \leq n \leq 2.0$	$Q^* > 0$	Real
Type 2	$-2.0 \leq n < 0.6$	$Q^* > 0$	Real
	$1.1 < n \leq 2.0$	$Q^* < 0$	Real
	$-0.25 < n \leq 1.1$		Complex
Type 3	$-2.0 \leq n < 0$	$Q^* > 0$	Real
	$-2.0 \leq n \leq 2.0$	$Q^* < 0$	Complex

Figure 8 shows the effect of the gradient index n on the critical heat flux Q^* for different values of the dimensionless thermal contact resistance R^*. When the heat flux transmits into the less distortive material (i.e., the FGM half-plane, $Q^* > 0$), the critical heat flux increases with the increases of the thermal contact resistance; and the contact is very stable when the gradient index $n \geq 0$. When the heat flux transmits into the more distortive material (i.e., the homogeneous half-plane, $Q^* < 0$), the system exhibits the complex root instability, and the absolute value of the critical heat flux increases with the increase of the thermal contact resistance.

4.4 Comparison between three types of material combinations

Figure 9 compares the effects of the gradient index n on the critical heat flux Q^* for three types of material combinations with $R^* = 1.0$. For positive heat flux, Types 1, 2 and 3 exhibit the real root instability, and Type 3 material combination leads to the maximum critical heat flux. Therefore, Type 3 material combination has the best performance on the thermoelastic instability among these material combinations for positive heat flux. However, for the negative heat flux, both complex and real roots can cause the instability for Types 2 and 3, while Type 1 will not exhibit instability. And also, the maximum critical heat flux of Type 2 is larger than that of Type 3.

Table 2 sums up the stability behavior for the static thermoelastic contact of three types of material combinations with $R^* = 1.00$. It is found that the gradient index has a significant effect on the stability behavior of the system. Both complex and real roots can cause the instability for a certain range of gradient index n for types 2 and 3, while only real root instability occurs for Type 1 when n is in the range from -2 to 2. For the three types of material combinations, it is obvious that the effect of the gradient index n on the present system is totally different from that on the system of an FGM layer on a homogeneous half-plane reported by Mao et al. [25] (please refer to Table 2 in Ref. [25]).

4.5 Comparison of the stability behavior with Mao et al. [25]

In this subsection, we give a detailed comparison of the stability behavior between the present paper and Mao et al. [25] for Types 1, 2 and 3 material combinations. Mao et al. [25] considered the thermoelastic instability between an FGM layer and a homogeneous half-plane (system I), while the present paper considers the thermoelastic instability between an FGM half-plane and a homogeneous half-plane (system II).

Figure 10 shows the comparison of the stability boundaries of the two systems for Type 1 material combination with the gradient index $n = 0.50$. For system II, only the real root instability can occur. System I, however, can exhibit both complex and real root instabilities for the small thickness and only real root instability for the large thickness. It is observed that the stability boundaries of system II are nearly the same as those of system I when the thickness of the FGM layer $H \geq 5.50$.

Figure 11 gives the comparison of the stability boundaries of the two systems for Type 2 material combination with the gradient index $n = 0.20$. System II can exhibit only the real root instability for the positive heat flux and only the complex root instability for the negative heat flux. System I, however, can exhibit both complex and real root instabilities for both directions of the heat flux at a certain thickness. If the thickness range is $H \geq 5.50$, the two systems can give the same solution.

Figure 12 presents the comparison of the stability boundaries of the two systems for Type 3 material combination with the gradient index $n = 0.50$. For system II, both complex and real root instabilities can occur for the negative heat flux, while the critical heat flux is determined from the complex root instability. For system I with small thickness of the FGM layer ($H = 1.00$), it can exhibit the complex root instability for

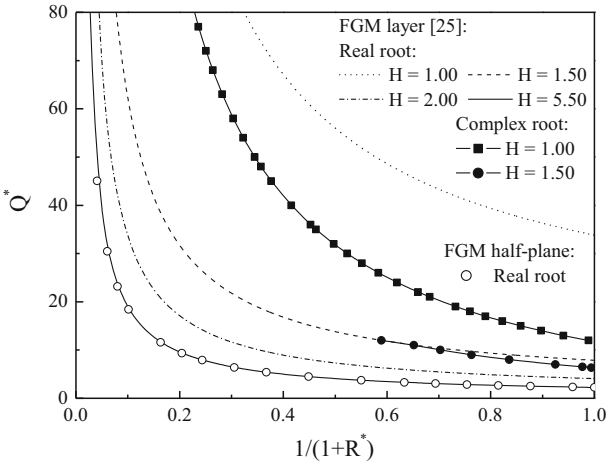

Fig. 10 Comparison of the stability boundaries of the two systems for Type 1 material combination with the gradient index $n = 0.50$

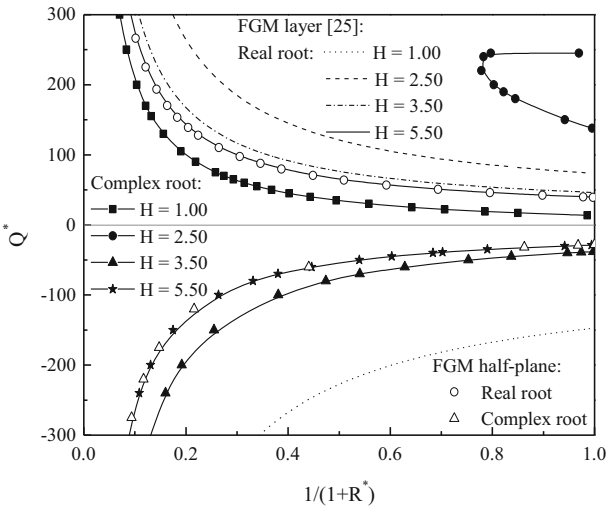

Fig. 11 Comparison of the stability boundaries of the two systems for Type 2 material combination with the gradient index $n = 0.20$

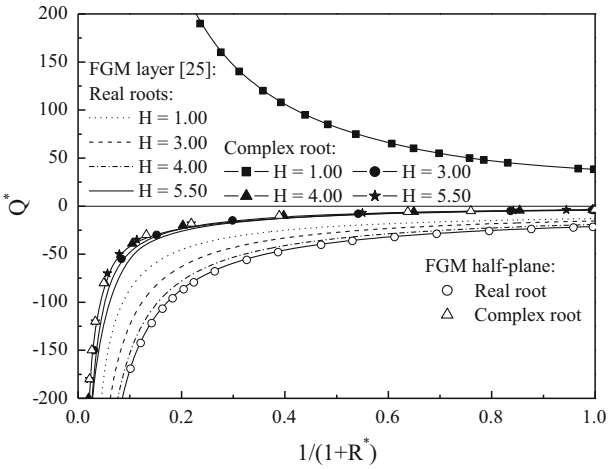

Fig. 12 Comparison of the stability boundaries of the two systems for Type 3 material combination with the gradient index $n = 0.50$

the positive heat flux and the real root instability for the negative heat flux. Similar to Types 1 and 2 material combinations, the two systems for Type 3 material combination can give the same solution when $H \geq 5.50$.

5 Conclusions

By using the perturbation method, this paper investigates the static thermoelastic contact instability of an FGM half-plane and a homogeneous half-plane under the plane strain state. Two frictionless half-planes are pressed together by a uniform pressure and transmit a uniform heat flux at their interface. The characteristic equation is obtained to determine the stability boundary for three types of material combinations. The effects of the gradient index and material combination on the critical heat flux and stability boundaries are discussed in detail. The results of the present analysis are validated by reducing the problem to the contact between two homogeneous half-planes. It is found that:

1. Instability only occurs when the heat flux flows into the material with larger distortivity for Type 1 material combination, while it could occur at both directions of the heat flux for Types 2 and 3 material combinations.
2. For all three types, the absolute value of the critical heat flux Q^* increases significantly with the increase of the thermal contact resistance.
3. Type 3 material combination has the best performance on the thermoelastic instability among these material combinations for the positive heat flux, while Type 1 material combination has the best performance for the negative heat flux.
4. The results indicate that we can increase the critical heat flux and change the stability boundaries by adjusting the gradient index of FGMs, and hence improve the thermoelastic stability behavior of systems.

Acknowledgments The work described in this paper is supported by National Natural Science Foundation of China under Grant numbers 11272040, 11322218 and 11411130173, Program for New Century Excellent Talents in University under Grant number NCET-13-0656.

Appendix A

$$\{g_{1i}\} = \{f_{11} - ms_1,\, f_{12} - ms_2,\, \frac{M_2}{M_1} + \eta_{11} + \gamma\ ,\, 0,\, 0,\, 0\}^{\mathrm{T}}, \tag{A1}$$

$$\{g_{2i}\} = \{0,\, 0,\, 0,\, 2m,\, 1 - \Theta_2,\, 2\eta_{21}\}^{\mathrm{T}}, \tag{A2}$$

$$\{g_{3i}\} = \left\{\frac{\mu_{\mathrm{b}}}{\Theta_1 - 1} L_1,\, \frac{\mu_{\mathrm{b}}}{\Theta_1 - 1} L_2,\, \mu_{\mathrm{b}} W,\, 2m\mu_2,\, -\left(\Theta_2 + 1\right)\mu_2,\, 2m\mu_2\right\}^{\mathrm{T}}, \tag{A3}$$

$$\{g_{4i}\} = \left\{s_1,\, s_2,\, -\frac{M_2}{mM_1},\, 1,\, -\frac{\Theta_2}{m},\, \frac{\eta_{21}}{m}\right\}^{\mathrm{T}}, \tag{A4}$$

$$\{g_{5i}\} = \left\{0,\, 0,\, \frac{k_{\mathrm{b}}\left(\Theta_1 - 1\right)\eta_{11}}{\bar{\alpha}_1 M_1},\, 0,\, 0,\, -\frac{k_2\eta_{21}\left(\Theta_2 + 1\right)\left(\eta_{21}^2 - m^2\right)}{\bar{\alpha}_2}\right\}^{\mathrm{T}}, \tag{A5}$$

$$\begin{aligned}\{g_{6i}\} = \Bigg\{&0,\, 0,\, -\frac{\Theta_1 - 1}{4\bar{\alpha}_1 mM_1},\, 2mq_0\mu_2 R',\\ &-q_0\mu_2\left(1 + \Theta_2\right)R',\, \frac{\left(1 + \Theta_2\right)\left(1 + \eta_{21}k_2R_0\right)\left(\eta_{21}^2 - m^2\right)}{4m\bar{\alpha}_2} + 2mq_0\mu_2R'\Bigg\}^{\mathrm{T}},\end{aligned} \tag{A6}$$

where

$$W = \frac{1}{mM_1} - \frac{\left(\Theta_1 + 1\right)M_2\left(\gamma + \eta_{11}\right)}{m\left(\Theta_1 - 1\right)M_1} - \frac{m\left(\Theta_1 - 3\right)}{\Theta_1 - 1}, \quad W^* = \frac{1}{M_1^*} - \frac{\left(\Theta_1 + 1\right)M_2^*\left(\gamma^* + \eta_{11}^*\right)}{\left(\Theta_1 - 1\right)M_1^*} - \frac{\Theta_1 - 3}{\Theta_1 - 1},$$

$$L_j = s_j f_{1j}\left(\Theta_1 + 1\right) - m\left(\Theta_1 - 3\right), \quad L_j^* = s_j f_{1j}^*\left(\Theta_1 + 1\right) - \left(\Theta_1 - 3\right), \quad j = 1, 2.$$

Appendix B

$$C_1(H,z) = (\Theta_1 - 1)\,\eta_{11}^* r_2 \left(\eta_{21}^* - 1\right)\left[(\Theta_1 + 1)r_4 + (\Theta_2 + 1)\right]\left[(s_2 - f_{12}^*)L_1^* - \left(s_1 - f_{11}^*\right)L_2^*\right]$$
$$+2\eta_{21}^* r_3 \left({\eta_{21}^*}^2 - 1\right)\left[1 + \Theta_2 + r_4\,(1 + \Theta_1)\right]\left[(\Theta_1 - 1)\left(f_{12}^* s_1 - f_{11}^* s_2\right) + M_1^* F_1 + M_2^* F_2\right], \quad \text{(B1)}$$

$$C_2(H,z) = 4\,(\Theta_1 - 1)^2\,\eta_{11}^*\eta_{21}^*\left({\eta_{21}^*}^2 - 1\right) r_3 r_4\left[\left(f_{12}^* - s_2\right)s_1 - (f_{11}^* - s_1)s_2\right]$$
$$+ (\Theta_1 - 1)\,(\Theta_2 + 1)\,\eta_{11}^*\eta_{21}^*\left(\eta_{21}^* - 1\right)\left(1 + \eta_{21}^* r_3\right)\left[\left(s_2 - f_{12}^*\right)L_1^* - \left(s_1 - f_{11}^*\right)L_2^*\right] \quad \text{(B2)}$$

where

$$F_1 = (\Theta_1 + 1)\left(f_{11}^* - f_{12}^*\right)\left(\eta_{11}^* + \gamma^*\right)s_1 s_2 + (3 - \Theta_1)\left[\left(f_{12}^* s_1 - f_{11}^* s_2\right) + (s_2 - s_1)\left(\eta_{11}^* + \gamma^*\right)\right],$$
$$F_2 = (\Theta_1 + 1)\left[f_{11}^* f_{12}^*\,(s_1 - s_2) - \left(\eta_{11}^* + \gamma^*\right)\left(f_{12}^* s_1 - f_{11}^* s_2\right)\right] + (\Theta_1 - 3)\left(f_{11}^* - f_{12}^*\right).$$

References

1. Suresh, S., Mortensen, A.: Functionally graded metals and metal-ceramic composites: part 2 thermomechanical behaviour. Int. Mater. Rev. **42**, 85–116 (1997)
2. Suresh, S.: Graded materials for resistance to contract deformation and damage. Science **292**, 2447–2451 (2001)
3. Ke, L.L., Wang, Y.S.: Two-dimensional contact mechanics of functionally graded materials with arbitrary spatial variations of material properties. Int. J. Solids Struct. **43**, 5779–5798 (2006)
4. Ke, L.L., Wang, Y.S.: Two-dimensional sliding frictional contact of functionally graded materials. Eur. J. Mech. A Solids **26**, 171–188 (2007)
5. Guler, M.A., Erdogan, F.: Contact mechanics of graded coatings. Int. J. Solids Struct. **41**, 3865–3889 (2004)
6. Guler, M.A., Erdogan, F.: Contact mechanics of two deformable elastic solids with graded coatings. Mech. Mater. **38**, 633–647 (2006)
7. Guler, M.A., Erdogan, F.: The frictional sliding contact problems of rigid parabolic and cylindrical stamps on graded coatings. Int. J. Mech. Sci. **49**, 161–182 (2007)
8. El-Borgi, S., Abdelmoula, R., Keer, L.: A receding contact plane problem between a functionally graded layer and a homogeneous substrate. Int. J. Solids Struct. **43**, 658–674 (2006)
9. Elloumi, R., Kallel-Kamoun, I., El-Borgi, S.: A fully coupled partial slip contact problem in a graded half-plane. Mech. Mater. **42**, 417–428 (2010)
10. Aizikovich, S.M., Vasilev, A.S., Krenev, L.I., Trubchik, I.S., Seleznev, N.M.: Contact problems for functionally graded materials of complicated structure. Mech. Compos. Mater. **47**, 539–548 (2011)
11. Chen, P.J., Chen, S.H., Peng, Z.: Thermo-contact mechanics of a rigid cylindrical punch sliding on a finite graded layer. Acta Mech. **223**, 2647–2665 (2012)
12. Chen, P.J., Chen, S.H.: Partial slip contact between a rigid punch with an arbitrary tip-shape and an elastic graded solid with a finite thickness. Mech. Mater. **59**, 24–35 (2013)
13. Choi, C.J., Paulino, G.H.: Thermoelastic contact mechanics for a flat punch sliding over a graded coating/substrate system with frictional heat generation. J. Mech. Phys. Solids **56**, 1673–1692 (2008)
14. Barik, S.P., Kanoria, M., Chaudhuri, P.K.: Steady state thermoelastic contact problem in a functionally graded material. Int. J. Eng. Sci. **46**, 775–789 (2008)
15. Shahzamanian, M.M., Sahari, B.B., Bayat, M., Ismarrubie, Z.N., Mustapha, F.: Transient and thermal contact analysis for the elastic behavior of functionally graded brake disks due to mechanical and thermal loads. Mater. Design **31**, 4655–4665 (2010)
16. Shahzamanian, M.M., Sahari, B.B., Bayat, M., Ismarrubie, Z.N., Mustapha, F.: Finite element analysis of thermoelastic contact problem in functionally graded axisymmetric brake disks. Compos. Struct. **92**, 1591–1602 (2010)
17. Liu, J., Ke, L.L., Wang, Y.S.: Two-thermoelastic contact problem of functionally graded materials involving frictional heating. Int. J. Solids Struct. **48**, 2536–2548 (2011)
18. Liu, J., Ke, L.L., Wang, Y.S., Yang, J., Alam, F.: Thermoelastic frictional contact of functionally graded materials with arbitrarily varying properties. Int. J. Mech. Sci. **63**, 86–98 (2012)
19. Chen, P.J., Chen, S.H.: Thermo-mechanical contact behavior of a finite graded layer under a sliding punch with heat generation. Int. J. Solids Struct. **50**, 1108–1119 (2013)
20. Li, C.: Thermoelastic Contact Stability Analysis, Ph.D. thesis. University of Michigan, Michigan (1998)
21. Jang, Y.H., Ahn, S.H.: Frictionally-excited thermoelastic instability in functionally graded material. Wear **262**, 1102–1112 (2007)
22. Lee, S., Jang, Y.H.: Effect of functionally graded material on frictionally excited thermoelastic instability. Wear **266**, 139–146 (2009)
23. Lee, S., Jang, Y.H.: Frictionally excited thermoelastic instability in a thin layer of functionally graded material sliding between two half-panes. Wear **267**, 1715–1722 (2009)
24. Hernik, S.: Modeling FGM brake disk against global thermoelastic instability (hot-spot). Z. Angew. Math. Mech. **89**, 88–106 (2009)
25. Mao, J.J., Ke, L.L., Wang, Y.S.: Thermoelastic contact instability of a functionally graded layer and a homogeneous half-plane. Int. J. Solids Struct. **51**, 3962–3972 (2014)
26. Lee, K., Barber, J.R.: Frictionally excited thermoelastic instability in automotive disk brakes. J. Tribol. **115**, 607–614 (1993)

27. Yi, Y.B., Barber, J.R., Zagrodzki, P.: Eigenvalue solution of thermoelastic instability problems using Fourier reduction. Proc. R. Soc. Lond. Ser. A Math. Phys. Eng. Sci. **456**, 2799–2821 (2000)
28. Lee, K.: Frictionally excited thermoelastic instability in automotive drum brakes. J. Tribol. **122**, 849–855 (2000)
29. Afferrante, L., Ciavarella, M., Decuzzi, P., Demelio, G.: Thermoelastic instability in a thin layer sliding between two halfplanes: transient behavior. Tribol. Int. **36**, 205–212 (2003)
30. Ahn, S.H., Jang, Y.H.: Frictionally excited-elastoplastic instability. Tribol. Int. **43**, 779–784 (2010)
31. Barber, J.R.: Stability of thermoelastic contact. Inst. Mech. Eng. Int. Conf. Tribol. **981**(-986), 981–986 (1987)
32. Zhang, R., Barber, J.R.: Effect of material properties on the stability of static thermoelastic contact. J. Appl. Mech. **57**, 365–369 (1990)
33. Yeo, T., Barber, J.R.: Stability of thermoelastic contact of a layer and a half-plane. J. Therm. Stress. **14**, 371–388 (1991)
34. Li, C., Barber, J.R.: Stability of thermoelastic contact of two layers of dissimilar materials. J. Therm. Stress. **20**, 169–184 (1997)
35. Afferrante, L., Ciavarella, M.: Frictionally excited thermoelastic instability in the presence of contact resistance. J. Strain Anal. Eng. Design **39**, 351–357 (2004)
36. Afferrante, L., Ciavarella, M.: Instability of thermoelastic contact for two half-planes sliding out-of-plane with contact resistance and frictional heating. J. Mech. Phys. Solids **52**, 1527–1547 (2004)
37. Ciavarella, M., Barber, J.R.: Stability of thermoelastic contact for a rectangular elastic block sliding against a rigid wall. Eur. J. Mech. A Solids **24**, 371–376 (2005)
38. Dundurs, J.: Distortion of a body caused by free thermal expansion. Mech. Res. Commun. **1**, 121–124 (1974)